Applied Energy 183 (2016) 408–418

Contents lists available at ScienceDirect

Applied Energy

journal homepage: www.elsevier.com/locate/apenergy

On the auxiliary boiler sizing assessment for solar driven supercritical CO_2 double recompression Brayton cycles

F.A. Al-Sulaiman

Center of Research Excellence in Renewable Energy (CoRERE), Research Institute, King Fahd University of Petroleum & Minerals (KFUPM), Dhahran 31261, Saudi Arabia

HIGHLIGHTS

- Monthly energy and exergy analyses of the solar driven sCO_2 Brayton system were conducted.
- The analyses were conducted for three power outputs.
- Monthly variations of heat fractions from the system components during day and night time were evaluated.
- Monthly assessment of the solar multiple for day and night time is presented.
- Detailed exergy analysis was conducted for both the solar system and sCO_2 Brayton system.

ARTICLE INFO

Article history:
Received 18 June 2016
Received in revised form 15 August 2016
Accepted 28 August 2016

Keywords:
Solar thermal power tower
Auxiliary boiler
Central receiver
Solar multiple
Supercritical CO_2 Brayton cycle
Exergy efficiency

ABSTRACT

A performance assessment of sizing an auxiliary boiler for a solar driven supercritical double recompression CO_2 Brayton cycle was conducted. The Brayton cycle is designed to deliver three different power outputs and the required size of the auxiliary boiler was examined in detail. The heat fraction to be delivered from the solar field and from the auxiliary boiler for each month of the year are reported. Furthermore, the daytime solar multiple and the twenty-four hour solar multiple were examined. Another key parameter that was studied is the effect of the turbine inlet temperature on the net power, energy efficiency, and exergy efficiency. Among the other exergy parameters that were examined are exergy destruction, exergy improvement potential, fuel depletion ratio, relative irreversibility, and productivity lack. The power output for Case 1, Case 2, and Case 3 is about 41.5 MW, 60.0 MW, and 90.0 MW, respectively; and for the month of June, the fraction of the heat from the auxiliary boiler during daytime hours is about 0.25, 0.40, and 0.54, respectively. For the three Cases the overall system energy efficiency during the month of June is 20.7%, 25.0%, 29.6%, and the overall system exergy efficiency is 22.2%, 28.3%, and 35.7%, respectively. The cycle efficiency is about 47% for the baseline conditions. In addition, the lowest thermal heat collected in the receiver is during December and, therefore, during this month, the highest auxiliary heat is required from the boiler. The 24-h average solar multiple for Case 1, Case 2, and Case 3 is 0.437, 0.303, and 0.202, respectively; and the average daytime solar multiple for these cases is 0.858, 0.590, and 0.396, respectively. Moreover, similar results are reported for each month of the year. Furthermore, the findings demonstrate that the heliostat has the highest exergy destruction rate and, thus, it has the highest exergy improvement potential.

1. Introduction

As solar energy is expected to be one of the most dominant utilized energy sources in the future, there is a crucial need to develop solar driven systems with improved performance. Solar thermal power tower technology, which can provide high temperature fluid and can be integrated with medium and large scale power plants, is the most promising concentrating solar thermal system. Among the thermal power cycles, supercritical carbon dioxide (sCO_2) Brayton cycle is one of the most promising due to its relatively high thermal efficiency. Thus, the combination of solar thermal power tower technology with double recompression sCO_2 Brayton cycle was selected for this study.

Several studies have been conducted to evaluate the performance of solar driven thermal power cycles, e.g. [1–4]. Spelling et al. [1] discussed the performance of a combined cycle hybrid solar gas-turbines and its advantages as compared to simple gas turbine cycle. The authors also discussed the annual solar share

E-mail address: fahadas@kfupm.edu.sa

http://dx.doi.org/10.1016/j.apenergy.2016.08.169
0306-2619/

Nomenclature

A_h	total area of the heliostats, m^2
A_R	surface area of the central receiver, m^2
$C1$	compressor one
$C2$	compressor two
$C3$	compressor three
DH	heliostat diagonal, m
DLH	number of daylight hours
DM	characteristic diameter, m
DR	receiver diameter (cylindrical), m
$Ex_{in,}$	exergy into the system, kW
$Ex_{d,j}$	exergy destruction rate of any component "j", kW
$Ex_{d,total}$	exergy destruction rate of the whole system, kW
Ex_{solar}	total incident solar exergy rate on the heliostat, kW
Ex_{in}	exergy input rate, kW
$Ex_{net,}$	net exergy rate gained, kW
f_{aux}	heat fraction from the auxiliary boiler during daytime for 24 h of operation
$f_{aux,daytime}$	heat fraction from the auxiliary boiler during daytime
f_{night}	heat fraction from the auxiliary boiler during nighttime
f_{rec}	heat fraction from the receiver during daytime
F_{view}	radiation view factor
H	specific enthalpy, kJ/kg
h_{conv}	convective heat transfer coefficient at the central receiver, kW/m^2 K
H_{tower}	total height of the tower
HTR	high temperature recovery
I	incident normal radiation, kW/m^2
IP_i	improvement potential of any component "j", kW
LH	height of the heliostat, m
LR	receiver size, m
LTR	low temperature recovery
LW	width of the heliostat, m
$\dot{m}$	mass flow rate of sCO_2 in the Brayton cycle, kg/s
MTR	medium temperature recovery
Q_{aux}	auxiliary heat through the boiler, kW
Q_{conv}	rate of convection heat losses from the central receiver, kW
Q_{in}	heat input, kW
Q_{out}	energy rejection rate at the cooler of the Brayton cycle, kW
Q_{rad}	rate of radiation heat losses from the central receiver, kW
$Q_{loss,}$	net energy loss, kW
$Q_{net,}$	net heat, kW
Q_{night}	heat required at night time, kW
Q_{solar}	total incident solar radiation on the solar field, kW
Q_u	net useful energy rate gained at the central receiver, kW
SM	solar multiple for 24 h of operation
$SM_{daytime}$	solar multiple during daytime
T_{amb}	ambient temperature
THT	tower optical height or aim point height, m
T_R	temperature at the central receiver surface
T_{sun}	temperature of the outer surface of the sun
x_{mass}	fraction of mass flow rate through the sCO_2 cycle

Subscripts

aux	auxiliary boiler
$c1$	compressor one
$c2$	compressor two
$c3$	compressor three
$cool$	cooler
cyc	cycle
HTR	high temperature recovery
LTR	low temperature recovery
rec	receiver
sys	associated with the whole system
t	turbine

List of Greek symbols

α_R	absorptivity of the central receiver
χ	relative irreversibility
δ	fuel depletion ratio
ε	emissivity of the central receiver
η_{ex}	exergy efficiency
$\eta_{ex,\ sys}$	overall system exergy efficiency
η_{opt}	optical efficiency of the heliostat
$\eta_{th,R}$	thermal efficiency of the central receiver
η_{solar}	solar thermal efficiency
η_{sys}	overall system energy efficiency
σ	Stefan-Boltzmann constant
ΔT	CO_2 temperature difference between the receiver exit and the required input temperature to the turbine (°C)
ξ	productivity lack

of the proposed configuration. In a different study, Rau et al. [2] examined the annual energy yield of a hybrid solar power plant, considering four scenarios. They considered two thermal energy storage scenarios and two heliostat sizes. Maximum electricity production with the highest solar share was one of the main criteria applied to examine the plants. Grange et al. [3] studied the integration of thermal energy storage and a combustion chamber with a solar driven gas turbine. Their study focused on the effect of the operating conditions of the thermal energy storage, which is affected by the solar radiation, on the combustion chamber. Heide et al. [4] proposed a new configuration of the solar driven combined cycle. The air is heated using the solar tower before it enters the combustion chamber, yielding a higher solar share.

Other studies have examined the potential of integrating solar parabolic trough aided coal-fired power plants, e.g. [5–8]. Hou et al. [5] studied the performance of a solar aided coal-fired system for power production in which the solar field consists of parabolic troughs. They identified the range of the temperature in which the system can run in a save mode and identified the maximum allowable thermal output from solar energy and the minimum consumption rate of the coal. In a different study, Wu et al. [6] assessed the performance of solar aided coal-fired system for power production with a thermal energy storage system where the solar field consists of parabolic troughs. They found that the thermal energy storage system will smoothen the operation of the plant and, consequently, improves its efficiency. In a different study, Zhai et al. [7] studied the relationship between the solar energy share under a range of a direct normal radiation where the solar field was parabolic troughs. They identified the best flow rate of the heat transfer fluid as a function of the solar radiation. . In a different study, Bonadies et al. [8] presented a solar driven combined cycle with a large thermal energy storage system, in which the operating hours of the integrated system can reach 17 h.

Supercritical CO_2 Brayton cycles with thermal efficiencies that can reach 50% are promising thermal power cycles. Such a high efficiency is due to the compressor inlet pressure being just above the critical pressure of the CO_2 working fluid. Under this specific condition the specific heat and density of the working fluid are

very high and, hence, the required compressor input power is very low [9]. Furthermore, these types of cycles are relatively small as compared to Rankine cycles, and they can work under a wide range of turbine inlet temperatures, meanwhile, maintaining a relatively high efficiency [9].

Several studies have been conducted on solar driven sCO_2 Brayton cycles. However, in most of these studies it is assumed that the input heat to the cycle matches the attainable heat from the solar tower, without having a direct interaction between the solar tower and the thermal power cycle. That is, they studied different thermal power cycles assuming a source heat within the range of the attainable heat that can be obtained from a solar energy system without studying a solar energy system. Only a few studies have considered solar thermal power tower systems with a direct interaction with sCO_2 Brayton cycles, e.g. [9–16]

Chacartegui et al. [10] reported the performance of the solar tower integrated with calcium looping process and CO_2 cycle using thermochemical energy storage system. They found that the first law efficiency reaches 46% and the second law efficiency reaches 48%. Iverson et al. [11] examined the variation of the solar heat input on a sCO_2 split flow recompression Brayton cycle. They also studied the effect of cutting the thermal heat input by 50% and by 100% for short durations on the power conditions and determined that the thermal mass existing in the system can run the Brayton cycle for a short time. In a different study, Turchi [12] conducted a performance analysis of a sCO_2 recompression Brayton cycle and compared its performance with a helium Brayton cycle, supercritical steam Rankine cycle, and superheated Rankine steam cycle. It was concluded that sCO has a higher thermal efficiency as compared to the other three cycles. Ma and Turchi [13] recommended a small solar tower design for simplicity in the power block. Neises and Turchi [14] compared the performance of three supercritical CO_2 Brayton cycles when integrated with concentrating solar power systems. They reported that the partial-cooling cycle is more cost effective as compared with simple and recompression cycle. Muto et al. [15] compared the performance of supercritical CO_2 Brayton cycle with subcritical Brayton cycle when each one is integrated with concentrating solar system and they reported that the thermal efficiency for the supercritical cycle is around 48.9% while for the other cycle is around 45.3%. Osorio et al. [16] conducted an exergy analysis of the sCO_2 cycle with thermal energy storage. In particular, they examined the effect of varying the storage mass flow fraction between the cold and hot storage tanks and identified an optimum fraction of the mass flow rate without the need to increase the mass flow rate involving the tanks. Al-Sulaiman and Atif [9] compared the performance of different sCO_2 cycles, each integrated with a solar thermal power tower. In their study, they did not consider a thermal storage tank or an auxiliary boiler. The cycles considered were simple, precompression, regenerative, split expansion, and recompression sCO_2 Brayton cycles. They concluded that the recompression cycle has the best overall performance while the regenerative cycle has a relatively good comparable performance under specific operating conditions.

Only a limited number of studies have considered the integration of an auxiliary boiler with a solar driven thermal power tower system. Even fewer studies have examined the exergy performance of such a system. However, none of these studies have considered an integrated system of a solar thermal power tower with a double recompression sCO_2 Brayton cycle as done here. Moreover, an informative practical approach was employed with the aim of studying different scenarios of sizing a thermal driven power plant for a given solar thermal power tower, taking into consideration key performance and operating parameters. Furthermore, the study considered integrating double recompression supercritical CO_2 Brayton Cycle, which is a promising thermal power cycle that has high efficiency. The study also presents the assessment of the performance of a heliostat field and the heat collected from it for the city of Tabuk, Saudi Arabia, as an illustrative example. The study presents both energy and exergy analyses of the system considered, and incorporates three power outputs and compares the performance of each one. The fractions of heat source for the solar field and the auxiliary boiler were also assessed for each month of the year for the three power outputs. Moreover, the solar multiples for all the cases considered were evaluated, and the effect of turbine inlet temperature on key parameters was studied. Key exergy parameters, including exergy efficiency, exergy destruction rate, fuel depletion rate, productivity lack, irreversibility rate, and exergy improvement potential were also examined.

2. System description

The integrated solar power system consists of a heliostat field, solar tower, auxiliary boiler, and supercritical CO_2 double recompression Brayton cycle, as shown in Fig. 1. In this study, three systems with different power outputs are analyzed: 41.5 MW, 60.0 MW, and 90.0 MW. The objective of this study is to assess the sizing requirements of an auxiliary boiler for a fixed heliostat size for the integrated systems examined through detailed energy and exergy analyses. The heliostat size is fixed and, hence, produces a limited thermal energy to operate the power cycle. Therefore, the auxiliary boiler is used to supplement the required thermal heat to maintain the required power output for each case considered, e.g. 41.5 MW, 60.0 MW, and 90.0 MW; and when there is no solar radiation, nighttime, the power demand will be delivered exclusively by the boiler. The demand for the power is during both daytime and night time and the system is designed to deliver the base load power requirements at fixed power output. Moisseytsev and Sienicki [17] conducted a parametric optimization study and, therefore, it was selected as a reference for validation, as discussed in the next section. The efficiency of compressor 1, compressor 2, and the turbine are 88.9%, 87.8%, and 93.4%, respectively [17]. The fractions of the mass flow rates of the CO_2 to compressor 1 is 0.21 and to compressor 2 is 0.11. These fractions were selected based on the optimization of the flow splitting of sCO_2 cycle as presented in their work [17]. The main characteristics of the solar field are given in Table 1. This study will provide the engineers and decision makers a detailed information on boiler sizing variation throughout the year for hybrid fossil-solar power systems.

3. Mathematical modeling

In modeling the system, mass, energy, and exergy balance equations were applied to each component of the system considered. The integrated solar thermal tower power system with the double recompression sCO_2 cycle is illustrated in Fig. 1. The modeling of the receiver and the equations used to model the heat fraction and the solar multiple, as well as the overall system performance are presented. The heliostat modeling and its optical efficiency considering an annual optimization of the heliostat was presented in another study by Atif and Al-Sulaiman [18,19], in which Matlab was used. Engineering Equation Solver was used to conduct this simulations. The modeling of the sCO_2 double recompression cycle was validated using the procedure described by Moisseytsev and Sienicki [17] employing the same operating conditions of their cycle. The validation of this study is demonstrated in Fig. 2. The current model shows excellent result as compared to literature. The system in this study refers to the complete system including

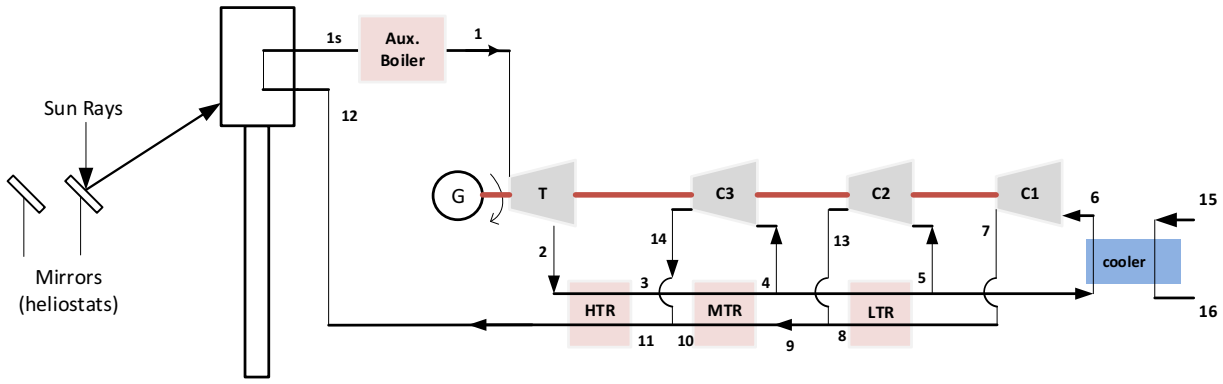

Fig. 1. Schematic diagram of the solar thermal power tower integrated with the double recompression cycle.

Table 1
Basic design and operating parameters used for the heliostat field and the central receiver [18,24–26].

Total number of heliostat, N_{hel}	2646
Receiver area, A_r	280 m^2
Tower optical height, *THT*	130 m
Heliostat height, *LH*	9.75 m
Heliostat width, *LW*	12.3 m
Fraction of mirror area of heliostat	0.9642
Receiver diameter (cylindrical), *DR*	9.44
Receiver size, *LR*	9.44
Mirror reflectivity × cleanliness, ρ	0.88 × 0.95
Standard deviation of sunshape errors, σ_{sun}	2.51 mrad
Standard deviation of tracking errors, σ_t	0.63 mrad
Standard deviation of beam quality errors, σ_{bq}	1.88 mrad
Total number of heliostats	2940
Emissivity of the receiver surface, ε	0.85
Absorptivity of the receiver surface, α_R	0.95
Receiver efficiency, $\eta_{th,r}$	0.80

the solar tower & heliostats and the supercritical CO_2 Brayton cycle while the cycle here is the supercritical CO_2 Brayton cycle, in which the auxiliary boiler and receiver are the heat input to the cycle.

3.1. Central receiver

The net heat rate from the receiver, which is the useful heat, equals,

$$Q_{net,solar} = \alpha_R Q_{in,solar} - Q_{loss,rec} \quad (1)$$

where α_R is the absorptivity of the receiver. The radiation back from the surroundings is very small as compared to the other terms and, therefore, it is neglected. The net energy intercepted at the receiver equals,

$$Q_{in,solar} = \eta_{opt}\ Q_{solar} \quad (2)$$

where η_{opt} is the heliostat optical efficiency. The total solar radiation incident on the heliostat equals,

$$Q_{solar} = IA_h \quad (3)$$

where I is the direct (beam) normal irradiation and A_h is the heliostat total area. The heat lost from the receiver is a function of both radiation heat and convection heat and it is equal to,

$$Q_{loss,rec} = Q_{rad} + Q_{conv} \quad (4)$$

The radiation heat losses from the central receiver is defined as [20],

$$Q_{rad} = F_{view} A \varepsilon \sigma T_R^4 \quad (5)$$

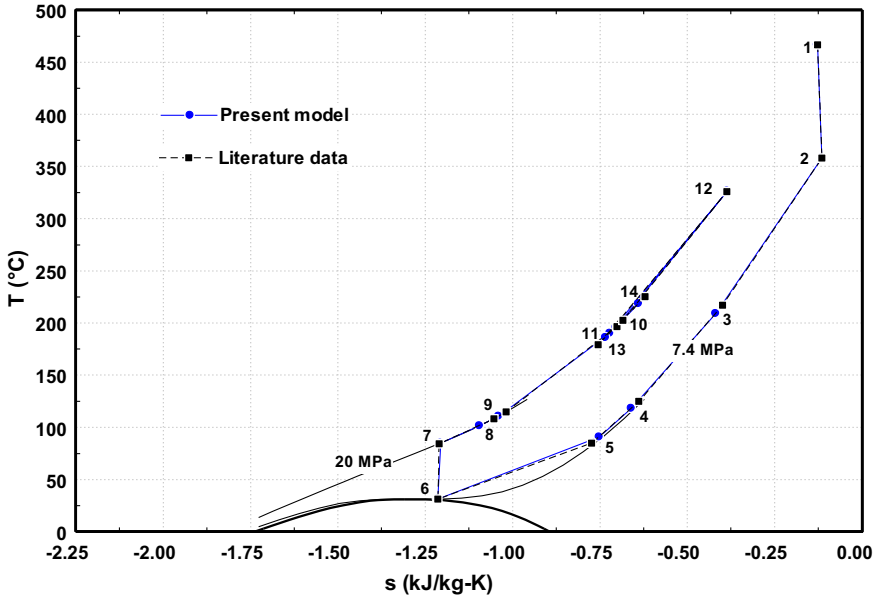

Fig. 2. Validation of the present model with literature [17].

where F_{view} is the radiation shape factor, A is the receiver radiative area, ε is the receiver emissivity, σ is the Stefan Boltzmann constant, and T_R is the temperature of the receiver. The convective heat losses from the central receiver is defined as,

$$Q_{conv} = A_R h_{conv}(T_R - T_{amb}) \tag{6}$$

where T_R is the average receiver temperature and T_{amb} is the ambient temperature. Here, h_{conv} was evaluated using the Bejan correlation for natural heat convection in a vertical chamber which is defined as [21],

$$h_{conv} = 0.557 \times 10^{-6}\left(\frac{T_R - T_{amb}}{H_t}\right)^{0.25} \text{ [kW/m}^2\text{ K]} \tag{7}$$

where H_t is the total height of the solar tower. The receiver type used in this study is cylindrical, in which the radiation received from all directions. The thermal efficiency of the receiver is defined as,

$$\eta_{th,R} = \frac{Q_{net,solar}}{Q_{in,solar}} \tag{8}$$

3.2. Exergy modeling of the system

Exergy analysis is associated with the maximum useful work that can be obtained from a system. Though different approaches can be used to calculate the exergy of a heliostat, the method presented by Petela [22] has received a wide acceptance. Using this method, the inlet exergy to the heliostat can be defined as,

$$Ex_{in,solar} = Q_{solar}\left(1 + \frac{1}{3}\left(\frac{T_{amb}}{T_{sun}}\right)^4 - \frac{4}{3}\left(\frac{T_{amb}}{T_{sun}}\right)\right) \tag{9}$$

where T_{sun} equals 5800 K. The exergy destructed by the heliostat can be defined as,

$$Ex_{d,solar} = (1 - \eta_{opt})Ex_{in,solar} \tag{10}$$

The total exergy into the system equals,

$$Ex_{in,total,sys} = Ex_{in,solar} + Ex_{in,aux} \tag{11}$$

The total exergy into the cycle equals,

$$Ex_{in,total,cyc} = Ex_{net,rec} + Ex_{in,aux} \tag{12}$$

The exergy parameters examined in this study are the exergetic improvement potential, fuel depletion ratio, irreversibility ratio, and the productivity lack. These modeling parameters are defined as follows.

The exergetic improvement potential identifies the component that has a high potential of improvement from an exergetic point of view. It is defined for a component j as,

$$IP_j = \left(1 - \frac{\eta_{ex,sys}}{100}\right)Ex_{d,j} \tag{13}$$

where $\eta_{ex,sys}$ is the exergy efficiency of the system as defined in Eq. (19). The exergetic fuel depletion ratio of the component j is defined as,

$$\delta_{d,j} = \frac{Ex_{d,j}}{Ex_{in,total,sys}} \tag{14}$$

The irreversibility ratio of the component j is defined as,

$$\chi_{d,j} = \frac{Ex_{d,j}}{Ex_{d,total}} \tag{15}$$

The productivity lack of the component j is defined as,

$$\xi_{d,j} = \frac{Ex_{d,j}}{W_{net}} \tag{16}$$

3.3. Overall system modeling

The overall system energy efficiency is defined as,

$$\eta_{sys} = \frac{W_{net}}{Q_{in,total}} \tag{17}$$

where $Q_{in,total}$ is the total heat into the system and is defined as,

$$Q_{in,total} = Q_{in,solar} + Q_{in,aux} \tag{18}$$

The overall system exergy efficiency is defined as,

$$\eta_{ex,sys} = \frac{W_{net}}{Ex_{in,total,sys}} \tag{19}$$

Considering 24 h of operation of the system, the fraction of the heat provided through the central receiver is defined as,

$$f_{rec} = \frac{Q_{net,rec}DLH}{Q_{net,rec}DLH + Q_{aux}DLH + Q_{night}(24 - DLH)} \tag{20}$$

where $Q_{net,rec}$ is the net heat from the receiver, Q_{aux} is the heat provided through the aux boiler during daytime, Q_{night} is the heat required during nighttime, and DLH is the number of daylight hours. The fraction of the heat provided through the auxiliary boiler is defined as,

$$f_{aux} = \frac{Q_{aux}DLH}{Q_{net,rec}DLH + Q_{aux}DLH + Q_{night}(24 - DLH)} \tag{21}$$

The fraction of the heat provided during nighttime is the heat required to keep the turbine at the rated capacity, which is defined as,

$$f_{night} = \frac{Q_{net,night}(24 - DLH)}{Q_{net,rec}DLH + Q_{aux}DLH + Q_{night}(24 - DLH)} \tag{22}$$

The fraction of the auxiliary heat during daytime is defined as,

$$f_{aux,daytime} = \frac{Q_{aux}}{Q_{net,rec} + Q_{aux}} \tag{23}$$

Other important parameter to assess the performance of the system considered is the solar multiple. Considering 24 h of operation of the system, it is defined as,

$$SM = \frac{Q_{net,rec}DLH}{Q_{net,cyc}24} \tag{24}$$

where $Q_{net,cyc}$ is the heat demand for the power block and it is equal to,

$$Q_{net,cyc} = m(h_1 - h_{12}) \tag{25}$$

where h is the specific enthalpy and m is the mass flow rate of CO_2. The solar multiple during daytime hours can be defined as,

$$SM_{daytime} = \frac{Q_{net,rec}}{Q_{net,cyc}} \tag{26}$$

The useful (net) solar thermal efficiency is a function of the net useful heat that can be used in the thermal power system. It is defined as,

$$\eta_{solar} = 100\frac{Q_{net,rec}}{Q_{solar}} \tag{27}$$

where the heat loss between the receiver and turbine inlet is negligible.

4. Results and discussion

In this section, the results of integrating the auxiliary boiler with the solar driven supercritical CO_2 Brayton cycles are

presented and discussed. First the solar radiation and the average monthly optical efficiency of the heliostat field for Tabuk city will be presented. The heliostat field was optimized for annual optical efficiency in another study by Atif and Al-Sulaiman [18,19]. Tabuk city was selected because it has high direct normal solar radiation and a potential of several large scale solar thermal power plants in Saudi Arabia. Next, the heats associated with the system considered will be evaluated and the operating conditions of the thermal cycle will be presented. Following which, the key parameters of the system including the heat fraction from the solar field and the auxiliary boiler, and the solar multiples will be examined for each month of the year for the three cases considered. The effect of the turbine inlet temperature on the power output, energy efficiency, and exergy efficiency will also be presented. Finally, several exergy parameters will be presented and discussed. The solar radiation variation has a negative impact on operating the supercritical CO_2 cycle and, therefore, an auxiliary boiler was included. This hybrid system will ensure uniform operation of the supercritical CO_2 cycle. The analysis considers three cases based on the net power outputs in the categories of small, medium, and large. Thus, the net power outputs are assumed as 41.5 MW, 60.0 MW, and 90.0 MW for Case 1, Case 2, and Case 3, respectively. For all three Cases the turbine inlet temperature is 580 °C, unless otherwise mentioned. The optimum solar field can produced a limited heat output during daytime hours. Therefore, Case 1 is considered when only minor heat input during daytime is needed from the auxiliary boiler, while the Case 2 is considered when around 40% of the heat input is supplied from the auxiliary boiler and for Case 3 is when around 60% of the heat input is supplied from the auxiliary boiler.

The solar field is designed to meet the heat requirement during June; and as will be demonstrated later in this section, the minimum heat input from the auxiliary boiler is during June.

4.1. Overall system analysis

The average monthly solar radiation and the optical efficiency of the heliostat field (Table 2) are two key parameters that provide information for both solar thermal power system designers and operators. Table 2 lists the average daily solar radiation, the number of daylight hours, the average hourly solar radiation during the daytime hours, and the optical efficiency of the heliostat field for each month. These values are used in the simulation in this study. One key observation from these data is that the average hourly solar radiation for the month of February is higher than several other months, such as March, although the average daily solar radiation is lower. This observation is attributed to the clear days usually in the month of February as compared to these months.

Table 3 lists the average data for several important variables. These variables are the average receiver temperature (T_R), the CO_2 exit temperature from the receiver (T_{1s}), the average received solar radiation to the heliostat field (Q_{solar}), average heat received by the receiver ($Q_{in,\ rec}$), average lost heat from the receiver ($Q_{loss,\ rec}$), average net heat within the receiver ($Q_{net,\ rec}$), average daily net heat within the receiver ($Q_{net,\ day,\ rec}$), average auxiliary heat (Q_{aux}), solar thermal efficiency (η_{solar}), and the system efficiency (η_{sys}). It is observed that the variations of these variables are directly related to the variation of the average solar radiation. For example, during the month of June, the need for the auxiliary boiler is minimal and the average required temperature to reach the turbine inlet temperature (580 °C) is 0.4 °C. The low temperature is attributed to the high thermal energy collected from the solar field, which is designed for this month of the year. Furthermore, for the month of June, the net heat collected in the receiver is the highest while the net heat required from the auxiliary boiler is the lowest. On the other hand, during the month of December, the required auxiliary heat is the highest, which is attributed to the low average solar radiation during this month. Moreover, it can be observed that the variation of the efficiency of the system is low, which is attributed to the assumed constant power output of the system throughout the year. Therefore, the variation of the solar radiation and the required auxiliary heat contribute directly to the thermal efficiency. The variation of the solar thermal efficiency is directly related to the net heat in the receiver and the solar radiation received by the heliostat field.

After assessing the overall system, it is necessary to determine the operating conditions of the system. The operating conditions of Case 1 with inlet turbine temperature of 580 °C during the month of June are given in Table 4.

Table 2
Solar radiation and heliostat efficiency [18].

Month	I_{day} (kW/m^2/day)	*DLH*	*I* (kW/m^2)	η_{opt}
1	6.17	10.5	0.5876	0.4705
2	6.86	11.2	0.6125	0.5701
3	7.19	12	0.5992	0.5429
4	7.44	12.8	0.5813	0.5192
5	7.88	13.5	0.5837	0.5436
6	9.12	13.9	0.6561	0.5525
7	8.86	13.7	0.6467	0.5487
8	8.24	13.1	0.6290	0.5306
9	7.59	12.3	0.6171	0.4962
10	6.34	11.5	0.5513	0.5201
11	6.0	10.7	0.5607	0.4804
12	5.8	10.3	0.5631	0.4593

4.2. Assessment of the fraction of the heat source

The fraction of the heat source for each month for the three Cases considered are illustrated in Fig. 3. The figure illustrates the fraction of the heat from the central receiver, from the auxiliary boiler during daytime, and the heat provided during nighttime from the auxiliary boiler. It is worth mentioning again that the size of the solar field is fixed for the three Cases and the extra demand for thermal heat is met completely by the auxiliary boiler, so that the turbine inlet temperature can be maintained constant. In addition, it should be noted that the fraction of the heat obtained from the central receiver is a function of both the solar radiation and the optical efficiency of the heliostat field. Table 2 illustrates these two parameters for each month, while Table 3 lists the heat collected in the receiver. From Fig. 3, it is observed that the contribution of heat from the central receiver decreases as the heat demand increases for Case 2 and Case 3 as compared to Case 1. Fig. 3a, demonstrates that there is almost no contribution from the auxiliary boiler during daytime in June, which is attributed to the size of the solar field that is designed for this Case and the solar multiple during daytime equals almost one. When there is more need to have power (Case 2 and Case 3 as compared to Case 1), the heat fraction from the auxiliary boiler increases as can be observed in Figs. 3b and 3c as compared to Fig. 3a. Note that the solar field size is fixed in this study as explained earlier.

The relative contribution of the auxiliary boiler during the daytime hours for the three Cases are plotted in Fig. 4 for each month. It can be observed that the contribution of the auxiliary boiler during daytime varies inversely with the net heat collected from the receiver for each month (Table 3).

4.3. Assessment of the solar multiple

The contribution of the net heat collected through the receiver is indicated by the daytime solar multiple data for each Case plotted in Fig. 5. The daytime solar multiple for Case 1 is the highest

Table 3
Monthly variation of key heat and temperature parameters and the system energy efficiency for Case1.

Month	T_R (°C)	T_{1s} (°C)	ΔT (°C)	Q_{solar} (kW)	$Q_{in,rec}$ (kW)	$Q_{loss,rec}$ (kW)	$Q_{net,\ rec}$ (kW)	$Q_{net,\ day,\ rec}$ (kW h/day)	Q_{aux} (kW)	$Q_{net,\ cyc}$ (kW)	η_{solar}	η_{sys}
1	711.7	543.6	36.44	179,789	84,591	12,689	67,672	710,561	21,279	88,951	37.64	20.66
2	770.9	574.1	5.949	187,401	106,838	16,026	85,470	957,264	3481	88,951	45.61	21.77
3	752.6	564.0	15.96	183,322	99,525	14,929	79,620	955,444	9331	88,951	43.43	21.57
4	733.5	554.2	25.81	177,840	92,335	13,850	73,868	945,506	15,084	88,951	41.54	21.54
5	746.2	560.7	19.30	178,591	97,082	14,562	77,666	1,048,000	11,286	88,951	43.49	21.88
6	780.7	579.6	0.40	200,746	110,912	16,637	88,730	1,233,000	222	88,951	44.20	20.67
7	775.1	576.4	3.578	197,870	108,571	16,286	86,857	1,190,000	2094	88,951	43.90	20.78
8	759.2	567.6	12.41	192,452	102,115	15,317	81,692	1,070,000	7259	88,951	42.45	20.80
9	737.2	556.0	23.96	188,801	93,683	14,052	74,946	921,839	14,005	88,951	39.70	20.49
10	720.7	547.9	32.13	168,678	87,729	13,159	70,183	807,110	18,768	88,951	41.61	22.16
11	705.3	540.6	39.42	171,567	82,421	12,363	65,937	705,522	23,014	88,951	38.43	21.35
12	695.4	536.1	43.94	172,289	79,132	11,870	63,306	652,050	25,645	88,951	36.74	20.99

Table 4
Operating conditions of the baseline conditions for Case 1 during the month of June.

Station	T (°C)	P (MPa)	h (kJ/kg)	s (kJ/kg K)	ex (kJ/kg)
1s	579.6	19.810	565.3	0.048	551.10
1	580.0	19.810	565.8	0.049	551.40
2	461.6	7.749	432.9	0.061	414.60
3	283.5	7.701	228.0	−0.256	306.10
4	130.5	7.668	53.67	−0.623	242.60
5	89.2	7.630	1.51	−0.758	231.60
6	31.3	7.400	−146.8	−1.214	221.50
7	85.0	20.000	−117.5	−1.205	248.00
8	110.5	19.970	−57.0	−1.042	259.00
9	118.9	19.970	−39.5	−0.997	262.80
10	268.5	19.940	181.3	−0.514	337.20
11	260.9	19.940	171.6	−0.531	333.00
12	426.6	19.880	376.5	−0.197	436.40
13	184.1	19.970	68.7	−0.740	293.30
14	232.8	19.940	135.3	−0.601	317.90
15	25.0	0.145	110.5	0.365	0.16
16	28.8	0.101	126.3	0.418	0.01

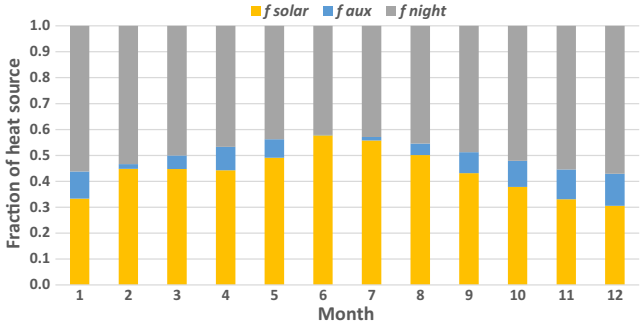

Fig. 3a. Fraction of the heat source for Case1.

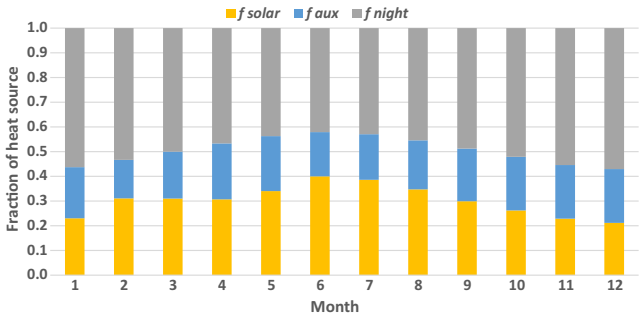

Fig. 3b. Fraction of the heat source for Case 2.

because the power output for this case is the lowest among the three Cases. In addition, the variation of the solar multiple for Case 1 is more than that for other two, again, due to the higher contribution of the heat provided by the receiver as compared to the other two Cases. The average daytime solar multiple for Case 1, Case 2, and Case 3 is about 0.85, 0.59, and 0.40, respectively.

Solar multiple can be defined for 24 h of operation to quantify the contribution of the net receiver heat for the total heat demand for the power block. Fig. 6 shows the solar multiple for 24 h of operation. The Figure shows that the solar multiple for Case 1, Case 2, and Case 3 varies between 0.58 and 0.30, 0.39 and 0.21, and 0.27

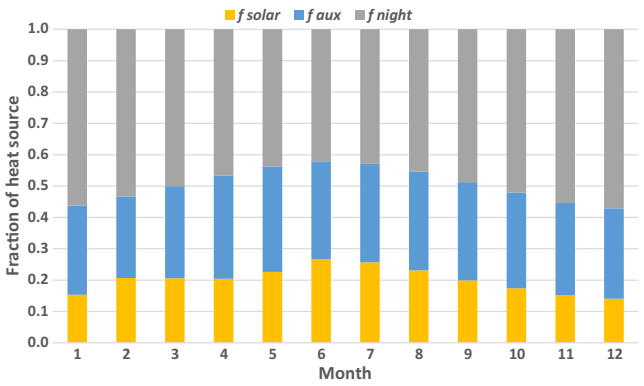

Fig. 3c. Fraction of the heat source for Case 3.

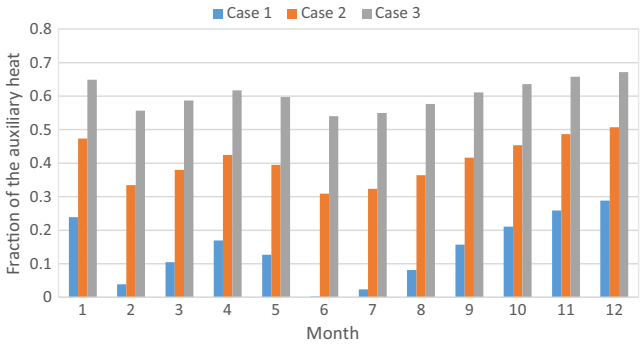

Fig. 4. Average of the fraction of the heat from the auxiliary boiler for the three Cases during daytime hours.

and 0.14, respectively. The average solar multiple for Case 1, Case 2, and Case 3 is about 0.44, 0.30, and 0.20, respectively.

4.4. Effect of the turbine inlet temperature

The most critical operating condition of the thermal power cycle is the turbine inlet condition. Figs. 7–9 illustrate the effect of the turbine inlet temperate on the net power output, energy efficiency, and exergy efficiency. Fig. 7 presents the net power output variation for the three Cases. For all three Cases, the temperature varies between 510 and 660 °C and the turbine inlet temperature increases as the net power output increases. As the inlet temperature increases the net power for Case 1, Case 2, and Case 3 increases from 36 MW to 47 MW, 52 MW to 68 MW, and 78 MW to 102 MW, respectively.

The turbine inlet temperature variation has a direct effect on the energy efficiency of the power system, as illustrated in Fig. 8. The figure shows that as the turbine inlet temperature increases as the energy efficiency increases. As the turbine inlet temperature increases, the energy efficiency for Case 1, Case 2, and Case 3 increases from 17 to 21%, 21 to 26%, and 25 to 31%, respectively. Case 3 has a higher system efficiency as a smaller fraction of the input power comes from the solar receiver as compared to the auxiliary boiler. That is, the solar power system has a lower thermal efficiency as compared to the auxiliary boiler. That is, Case 3 has a higher efficiency because power which figures in the numerator of the energy efficiency calculation increases and the solar radiation that falls on the heliostat and the heat provided through the auxiliary boiler which figure in denominator of the energy efficiency calculation decreases. The average optical efficiency of the heliostat is around 52%, indicating that a major

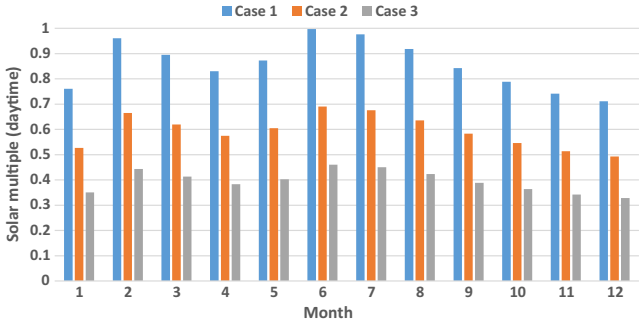

Fig. 5. Daytime solar multiple for the three Cases.

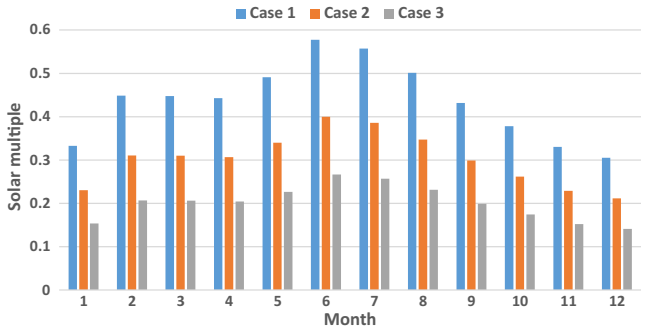

Fig. 6. Solar multiple for the three Cases.

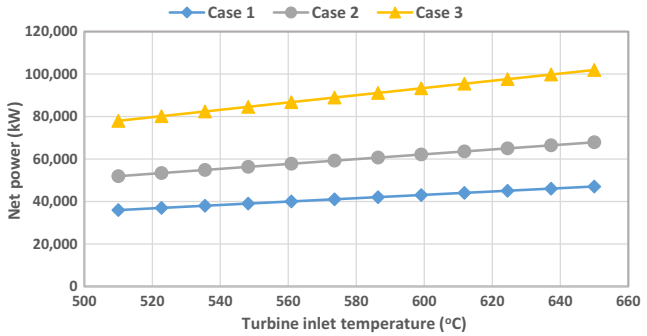

Fig. 7. Net power produced as a function of the variation of the turbine inlet temperature for the three Cases.

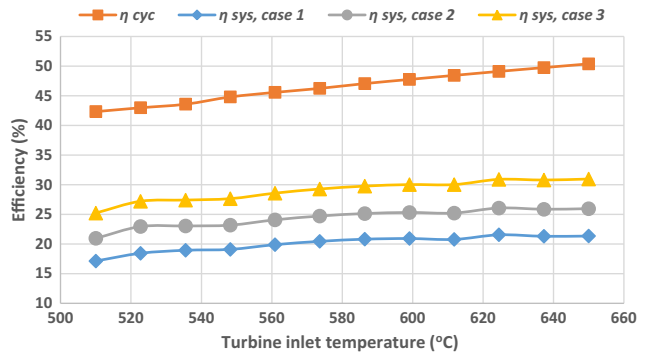

Fig. 8. Energy efficiency as a function of the variation of the turbine inlet temperature for the three Cases.

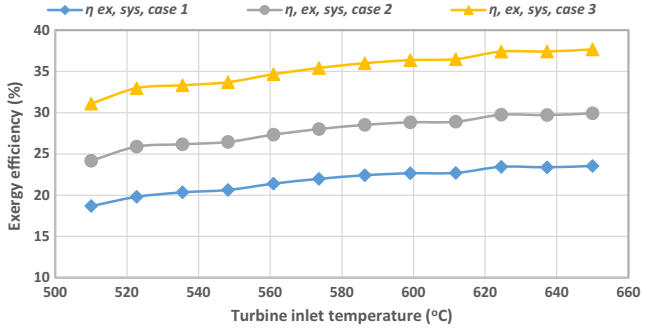

Fig. 9. Exergy efficiency as a function of the variation of the turbine inlet temperature for the three Cases.

portion of the heat is lost before it reaches the receiver. In addition, further heat is lost in the receiver, as illustrated by the data, especially the η_{solar} values, listed in Table 3. The net heat collected in the receiver is the same for all three Cases. On the other hand, the auxiliary boiler will provide the heat difference, with that provided in Case 1 being the lowest, while that provided in Case 3 being the highest. It should be noted that the sCO_2 cycle has relatively very high efficiency and this is maintained only if the inlet conditions to the compressor are maintained just above the critical conditions of the CO_2. (31.1 °C and 7.37 MPa). Under these operating conditions, the density of CO_2 is very high and, hence, the compressor requires relatively low power to increase the pressure to the required output. Therefore, the compressor inlet conditions should always be kept constant for sCO_2 cycles and just above the critical conditions. To control the compressor inlet temperature, a cooling system is used. The cooler includes a sCO_2 low pressure ratio compressor loop, an expansion valve, and a heat exchanger [23]

4.5. Exergy analysis

The variation of exergy efficiency as a function of the turbine inlet temperature for the three Cases are presented in Fig. 9. Reasoning similar to those used to explain the energy efficiency variations can be used to explain the variations of exergy efficiency. Exergy efficiency increases as the turbine inlet temperature increases from 510 to 660 °C. The observed increase of the exergy efficiency for Case 1, Case 2, and Case 3 is from 18.7 to 23.5%, 24.2 to 30.0%, and 31.0 to 37.7%, respectively.

The monthly exergy analysis of the exergy input to the system and the exergy efficiency of the system for Case 1, which varies between 22.2 and 24.6%, are given in Table 5. The variation of the solar exergy into the system and the receiver inlet exergy is consistent with the variation of the solar radiation given in Table 2. It can be noticed as the exergy fed from the solar energy increases, the exergy fed from the auxiliary boiler decreases. For example, when the exergy fed from the solar system is the highest, 186,763 kW, the exergy fed from the auxiliary boiler is the lowest, 142.8 kW. In order to meet the demand of exergy needed to operate the thermal power cycle, the exergy fed into the receiver and the exergy from the auxiliary boiler vary.

The exergy destruction analysis is an important tool that identifies and quantifies the amount of exergy destructed by each component. When the components with the highest exergy destruction are identified, further improvements can be made to decrease the exergy destruction by these components. Fig. 10 illustrates the results of the exergy destruction rate analysis for Case 1 for the month of June. The heliostat has the highest exergy destruction rate, which is around 83.6 MW and hence careful design of the heliostat is crucial to reduce exergy destruction. Other components contribute to 12.7 MW of the exergy destruction rate, with the turbine, HTR, MTR, and the cooler contributing high exergy destruction of 1.8 MW, 2.4 MW, 2.2 MW, and 3.7 MW, respectively.

Other key exergy parameters are exergy improvement potential (*IP*), fuel depletion ratio (δ), relative irreversibility (χ), and the productivity lack (ξ). In order to understand the variation of these parameters, it is necessary to look at the data for exergy fed into the system and the exergy destructed by all components. Exergy fed into the system and the exergy destructed by each component for the baseline conditions of the three Cases for the month of June are given in Table 6. It can be noticed that the rate of the total exergy fed into the cycle is the highest for Case 3 because the power produced for this case is the highest; similarly, the rate of the total exergy destructed is the highest for this case.

Exergy improvement potential is a key parameter that illustrates where and how much improvement is possible from an exergetic point of view (see Table 7). The findings demonstrate that the improvement potential for the solar field is the highest, with Case 1 having the highest potential, while Case 3 having the lowest potential because the contribution of the solar field is lowest for Case 3. Among the other components having a good improvement potential are the cooler, HTR, MTR, and LTR.

The exergetic fuel depletion ratio (δ) illustrates the relationship between the exergy destruction by a component as compared with the total exergy into the system. Table 8 lists the fuel depletion ratio of several components for the three Cases considered. It can be observed that the fuel depletion ratio for the heliostat, which is the highest, for Case 1, Case 2, and Case 3 is 0.4472, 0.3951, and 0.3327, respectively. Case 1 has the highest fuel depletion ratio of the heliostat because it has the highest solar multiple with high exergy destruction in the heliostat. Individual components of the cycle for Case 3 possess the highest fuel depletion ratios because it is the largest of the three Cases with the highest power output.

The irreversibility ratio of a component (χ) is defined as the ratio of the exergy destruction by the component as compared with the total exergy destructed. Table 9 lists the irreversibility ratios of the main components of the system. Trends similar to those observed for the fuel depletion ratio are also observed for this parameter. The irreversibility ratio of the heliostat is the highest, with Case 1 having the highest value (0.8678) while Case 3 the lowest value (0.7451).

The productivity lack (ξ) is defined as the ratio of the exergy destruction of a component as compared to the net power produced. Table 10 lists the productivity lack of various components

Table 5
Exergy into the system and system exergy efficiency for Case 1.

Month	$\eta_{ex,\ sys}$	$Ex_{\ in\ solar}$ (kW)	$Ex_{in,\ rec}$ (kW)	$Ex_{in,\ aux}$	$Ex_{in,total\ cyc}$ (kW)	$Ex_{in\ total\ sys}$ (kW)
1	22.98	167,266	41,260	13,555	54,815	180,821
2	23.53	174,348	52,111	2240	54,351	176,589
3	23.53	170,553	48,544	5985	54,529	176,538
4	23.73	165,453	45,037	9643	54,680	175,096
5	23.96	166,151	47,352	7231	54,583	173,382
6	22.23	186,763	54,098	142.8	54,241	186,906
7	22.40	184,088	52,956	1349	54,305	185,437
8	22.62	179,047	49,807	4662	54,469	183,709
9	22.51	175,650	45,694	8959	54,654	184,609
10	24.60	156,929	42,791	11,973	54,764	168,902
11	23.84	159,617	40,201	14,646	54,847	174,263
12	23.53	160,289	38,597	16,295	54,892	176,583

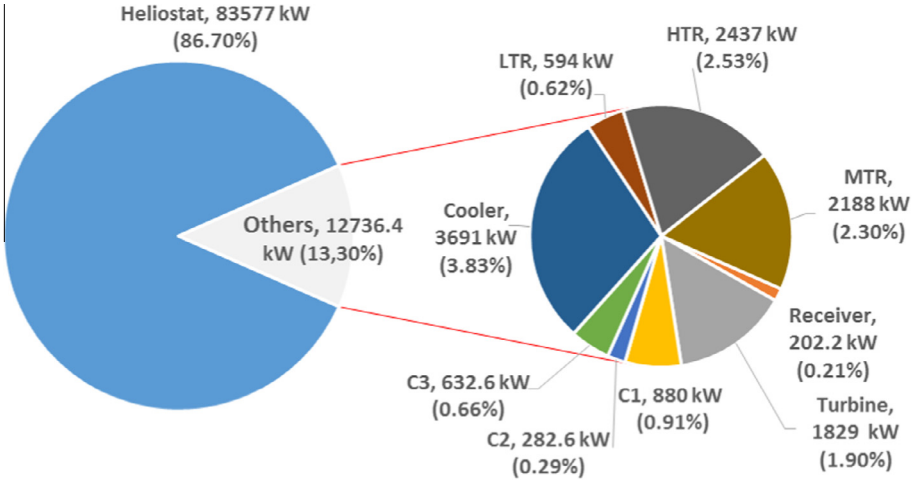

Fig. 10. Exergy destruction rate (kW) for the operating conditions of Table 4 for Case 1.

Table 6
Exergy in and exergy destructed for the three Cases under the baseline conditions for the month of June.

	Case 1 (kW)	Case 2 (kW)	Case 3 (kW)
$Ex_{solar\ in}$	186,763	186,763	186,763
$Ex_{in\ total\ cyc}$	54,241	78,589	118,271
$Ex_{in\ aux}$	143	24,765	64,447
$Ex_{in\ total\ sys}$	186,906	211,528	251,210
$Ex_{d\ solar\ helio}$	83,577	83,577	83,577
$Ex_{d\ rec}$	202	1277	2190
$Ex_{d\ t}$	1829	2641	3965
$Ex_{d\ c1}$	880	1271	1908
$Ex_{d\ c2}$	283	409	613
$Ex_{d\ c3}$	633	913	1370
$Ex_{d\ cool}$	3691	5167	7290
$Ex_{d\ LTR}$	594	852	1280
$Ex_{d\ HTR}$	2437	3436	5157
$Ex_{d\ MTR}$	2188	3193	4794
$Ex_{d\ total\ cyc}$	12,738	19,160	28,590
$Ex_{d\ total\ sys}$	96,314	102,736	112,166

Table 7
Exergy Improvement potential under the baseline conditions for the month of June.

	Case 1 (kW)	Case 2 (kW)	Case 3 (kW)
IP_{solar}	65,000	60,155	53,971
IP_{rec}	157	919	1414
IP_{aux}	0.01	0.56	15.00
IP_{c1}	684	915	1232
IP_{c2}	220	294	396
IP_{c3}	492	657	885
IP_{cooler}	2871	3719	4708
IP_{HTR}	1896	2473	3330
IP_{LTR}	462	614	826
IP_{MTR}	1702	2299	3096
IP_{t}	1423	1901	2560
IP_{total}	74,906	73,946	72,433

of the system for the three Cases considered. It can be noticed that the productivity lack of the heliostat, which is the highest, for Case 1, Case 2, and Case 3 is about 2.00, 1.40 and 0.94, respectively. The other components have significantly lower values.

Table 8
Fuel depletion ratio under the baseline condition for the month of June.

	Case 1	Case 2	Case 3
δ_{solar}	0.4472	0.3951	0.3327
δ_{rec}	0.0011	0.0060	0.0087
δ_{aux}	7.40E−08	3.67E−06	9.04E−05
δ_{c1}	0.0047	0.0060	0.0076
δ_{c2}	0.0015	0.0019	0.0024
δ_{c3}	0.0034	0.0043	0.0054
δ_{cool}	0.0198	0.0244	0.0290
δ_{HTR}	0.0130	0.0162	0.0205
δ_{LTR}	0.0032	0.0040	0.0051
δ_{MTR}	0.0117	0.0151	0.0191
δ_{t}	0.0098	0.0125	0.0158

Table 9
Relative irreversibility under the baseline conditions for the month of June.

	Case 1	Case 2	Case 3
χ_{solar}	0.8678	0.8135	0.7451
χ_{rec}	0.00210	0.0124	0.0195
χ_{aux}	1.44E−07	7.56E−06	0.0002
χ_{c1}	0.0091	0.0124	0.0170
χ_{c2}	0.0029	0.0040	0.0055
χ_{c3}	0.0066	0.0089	0.0122
χ_{cooler}	0.0383	0.0503	0.0650
χ_{HTR}	0.0253	0.0334	0.0460
χ_{LTR}	0.0063	0.0083	0.0114
χ_{MTR}	0.0227	0.0311	0.0427
χ_{t}	0.0190	0.0257	0.0354

Table 10
Productivity lack under the baseline condition for the month of June.

	Case 1	Case 2	Case 3
ξ_{solar}	2.0120	1.4100	0.9392
ξ_{rec}	0.0049	0.0215	0.0246
ξ_{aux}	3.33E−07	1.31E−05	0.0003
ξ_{c1}	0.0212	0.0214	0.0214
ξ_{c2}	0.0068	0.0069	0.0069
ξ_{c3}	0.0152	0.0154	0.0150
ξ_{cool}	0.0889	0.0872	0.0819
ξ_{HTR}	0.0587	0.0580	0.0580
ξ_{LTR}	0.0143	0.0144	0.0144
ξ_{MTR}	0.0528	0.0539	0.0539
ξ_{t}	0.0440	0.0445	0.0445

5. Conclusions

Energy and exergy analyses of a solar thermal power tower system integrated with a double recompression sCO_2 Brayton cycle were conducted. The study considered different power outputs in which an auxiliary boiler maintains a constant turbine inlet temperature.

Several important findings were presented and discussed. For example, for the month of June, the power output for Case 1, Case 2, and Case 3 is around 41.5 MW, 60.0 MW, and 90.0 MW, respectively, and the fraction of the heat from the auxiliary boiler during daytime hours is about 0.25, 0.40, and 0.54, respectively. The daytime solar multiple for the three Cases during the month of June is 1.00, 0.69, and 0.46, respectively. During the month of June the overall system energy efficiency for Case 1, Case 2, and Case 3 is 20.7%, 25.0%, 29.6%, respectively, while the overall system exergy efficiency is 22.2%, 28.3%, and 35.7%, respectively. Considering that the heliostat has the highest exergy destruction rate and the highest exergy improvement potential, improving the design of the heliostat is a key in the overall system design.

Acknowledgment

The author acknowledges the support of King Fahd University of Petroleum & Minerals (KFUPM), Dhahran, Saudi Arabia, for this work through project # SB121010.

References

[1] Spelling J, Laumert B, Fransson T. Advanced hybrid solar tower combined-cycle power plants, energy procedia. Energy Procedia 2014;49:1207–17.
[2] Rau C, Alexopoulos S, Breitbach G, Hoffschmidt B, Latzke M, Sattler J. Transient simulation of a solar-hybrid tower power plant with open volumetric receiver at the location Barstow. Energy Procedia 2014;49:1481–90.
[3] Grange B, Dalet C, Falcoz Q, Siros F, Ferrière A. Simulation of a hybrid solar gas-turbine cycle with storage integration. Energy Procedia 2014;49:1147–56.
[4] Heide S, Felsmann C, Gampe U, Boje S, Gericke B, Freimark M, Langnickel U, Buck R, Giuliano S. Parameterization of high solar share gas turbine systems. In: ASME Turbo Expo. Copenhagen, Denmark, GT2012-68608, June 11–15.
[5] Hou H, Wu J, Yang Y, Hu E, Chen S. Performance of a solar aided power plant in fuel saving mode. Appl Energy 2015;160:873–81.
[6] Wu J, Hou H, Yang Y, Hu E. Annual performance of a solar aided coal-fired power generation system (SACPG) with various solar field areas and thermal energy storage capacity. Appl Energy 2015;157:123–33.
[7] Zhai R, Zhao M, Tan K, Yang Y. Optimizing operation of a solar-aided coal-fired power system based on the solar contribution evaluation method. Appl Energy 2015;146:328–34.
[8] Bonadies MF, Mohagheghi M, Ricklick M, Kapat JS. Solar retrofit to combined cycle power plant with thermal energy storage. In: ASME, Paper No. GT2010-23685, Glasgow, UK, June 14–18; 2010.
[9] Al-Sulaiman FA, Atif M. Performance comparison of different supercritical carbon dioxide Brayton cycles integrated with a solar power tower. Energy 2015;82:61–71.
[10] Chacartegui R, Alovisio A, Ortiz C, Valverde JM, Verda V, Becerra JA. Thermochemical energy storage of concentrated solar power by integration of the calcium looping process and a CO_2 power cycle. Appl Energy 2016;173:589–605.
[11] Iverson BD, Conboy TM, Pasch JJ, Kruizenga AM. Supercritical CO_2 Brayton cycles for solar-thermal energy. Appl Energy 2013;111:957–70.
[12] Turchi C. Supercritical CO_2 for application in concentrating solar power systems. In: Proceedings of SCCO2 Power Cycle Symposium, Troy, NY, USA, April 2009.
[13] Ma Z, Turchi CS. Advanced supercritical carbon dioxide power cycle configurations for use in concentrating solar power systems. In: Proceedings of the Supercritical CO2 Power Cycle Symposium, Boulder, Colorado, USA, May 24–25.
[14] Neises T, Turchi C. Supercritical CO_2 power cycles: design considerations for concentrating solar power. In: The 4th international symposium – supercritical CO_2 power cycles, Pittsburgh, Pennsylvania, US; 2014 [paper# 75].
[15] Muto Y, Aritomi M, Ishizuka T, Watanabe N. Comparison of supercritical CO_2 gas turbine cycle and Brayton CO_2 gas turbine cycle for solar thermal power plants. In: The 4th International Symposium – Supercritical CO_2 Power Cycles, Pittsburgh, Pennsylvania, US.
[16] Osorio JD, Rivera-Alvarez A, Swain M, Ordonez JC. Exergy analysis of discharging multi-tank thermal energy storage systems with constant heat extraction. Appl Energy 2015;154:333–43.
[17] Moisseytsev A, Sienicki JJ. Performance improvement options for the supercritical carbon dioxide Brayton Cycle ANL-GenIV-103. Argonne National Laboratory; 2007.
[18] Atif M, Al-Sulaiman FA. Development of a mathematical model for optimizing a heliostat field layout using differential evolution method. Int J Energy Res 2015;39:1241–55.
[19] Atif M, Al-Sulaiman FA. Optimization of heliostat field layout in solar central receiver systems on annual basis using differential evolution algorithm. Energy Convers Manage 2015;95:1–9.
[20] Sheu EJ, Mitsos A. Optimization of a hybrid solar-fossil fuel plant: solar steam reforming of methane in a combined cycle. Energy 2013;51:193–202.
[21] Segal A, Epstein M. Comparative performances of tower-top and tower-reflector central solar receivers. Sol Energy 1999;65:207–26.
[22] Petela R. Exergy analysis of the solar cylindrical-parabolic cooker. Sol Energy 2005;79:221–33.
[23] Ahn Y, Bae SJ, Kim M, Cho SK, Baik S, Lee JI, Cha JE. Review of supercritical CO_2 power cycle technology and current status of research and development. Nucl Eng Technol 2015;47:647–61.
[24] Ho CK, Iverson BD. Review of high-temperature central receiver designs for concentrating solar power. Renew Sustain Energy Rev 2014;29:835–46.
[25] Collado FJ. Quick evaluation of the annual heliostat field efficiency. Sol Energy 2008;82:379–84.
[26] Collado FJ, Guallar J. A review of optimized design layouts for solar power tower plants with campo code. Renew Sustain Energy Rev 2013;20:142–54.